

Thermal and Imaging Correlation for the Validation of an MRI-guided Cryoablation Protocol

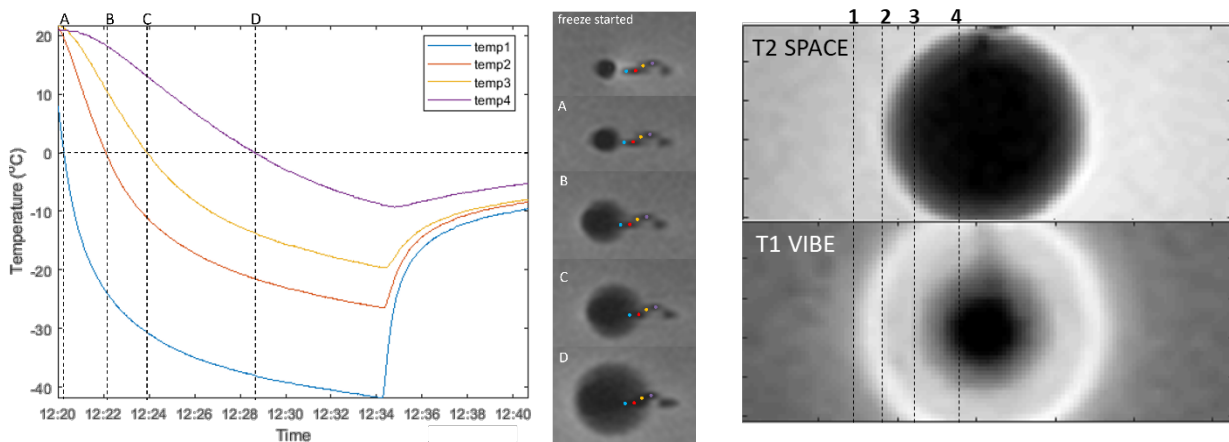
Mobeen Ali¹, Rory Heard¹, David J. Breen¹, Angela Darekar¹, Alexander J. King¹

¹University Hospital Southampton NHS Foundation Trust

Background. Percutaneous cryoablation is becoming increasingly accepted as a viable option for treating several tumour types, and in an array of clinical scenarios [1]. Much of the published cryoablation literature pertains to CT guided renal tumour ablation, but more recently is beginning to appear as an MRI guided procedure in selected settings [2]. MRI has several advantages over CT; no ionising radiation, better depiction of the ice ball, and often increased conspicuity of the target lesion and surrounding structures [3]. This notion is particularly pertinent in prostate cryoablation, where visible lesions can be targeted in a controlled manner, whilst sparing critical structures such as the rectal wall, urethra and neurovascular bundles. MRI is a powerful tool for observing changes in tissue. However, the MRI appearance of the developing iceball has had limited testing [4] and validation in a clinical MRI setting. In order to safely use MRI guided cryoablation as a therapeutic tool, we need to quantify the iceball signal void correlates in terms of tissue temperature. In this study, we aim to investigate whether the visible signal void truly corresponds to the volume of the underlying ice ball, and where the bright band observed in certain images lies in relation to the periphery of the ice.

Methods. Fiberoptic temperature probes and a cryo-needle were inserted into an ultrasound-gel filled phantom. The cryo-needle was activated whilst a TrueFISP dynamic sequence was acquired using a Siemens Aera 1.5T MRI scanner, to map the signal void as each temperature probe reached 0°C. 3D T1 VIBE and T2 SPACE sequences were acquired at the end of the freezing phase and registered against each other, to correlate features between the two images.

Results. Using TrueFISP images of the ice ball, the signal void edge consistently corresponded to 0°C measurements. The nearest probes either side of 0°C were 3mm apart, thus placing the ice edge within 1.5mm of the signal void edge. In T2 SPACE images, the signal void had a constant intensity and well-defined margins, which aligned with the inside edge of the bright rim on the registered T1 VIBE image. Thus, the bright rim likely represents a region of phase change.



Discussion. The temperature measurements highlighted a steep temperature gradient across the edge of the ice formation. The T2 SPACE and TrueFISP sequences can be used to accurately determine the edge of the ice ball, whereas T1 VIBE images help illustrate the regions of ice forming or thawing.

Conclusion. The ice edge was confirmed to match imaging representations in TrueFISP and T2 SPACE images and aligned with the inside edge of the bright rim in T1 VIBE images.

Key references.

- 1) Yilmaz S, et al. (2016) Use of cryoablation beyond the prostate. *Insights imaging*. 7: 223-232.
- 2) King AJ, et al. (2019) Establishing MRI-guided prostate intervention at a UK Centre. *Br J Radiol*. 92: 20180918.
- 3) Permpongkosol S, et al. (2006) Percutaneous renal cryoablation. *Urology*. 68: 19-25.
- 4) Gilbert JC, et al. (1997) Temperature determination in the frozen region during cryosurgery of rabbit liver using MR image analysis. *Magn Reson Imaging*. 15: 657-667.

QSM Observational Case Studies of Superficial Siderosis Patients Undergoing Chelation Therapy

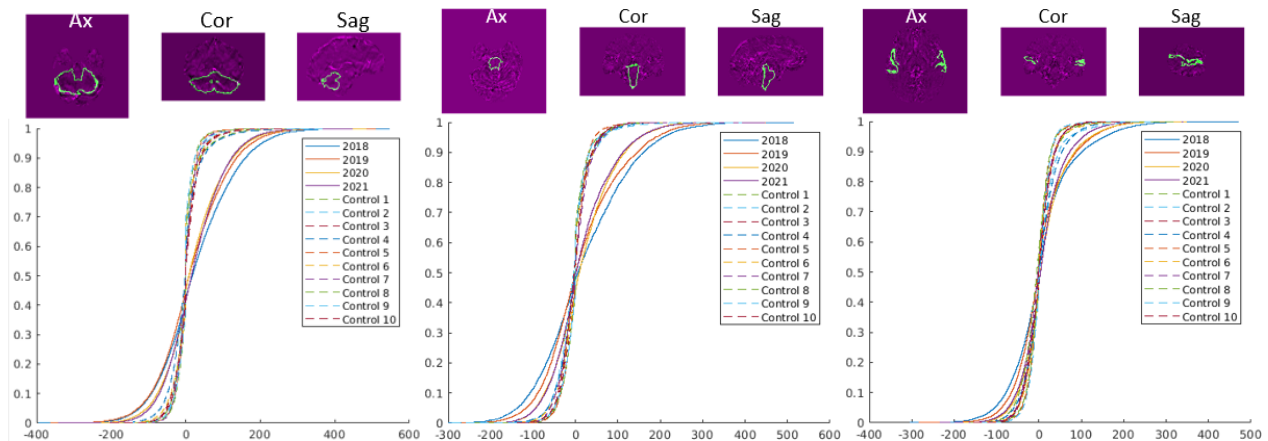
Mobeen Ali¹, Ardalan Zolnourian¹, Diederik Bulters¹, Ian Galea^{1,2}

¹University Hospital Southampton NHS Foundation Trust, ²University of Southampton

Background. Superficial siderosis (SS) of the central nervous system is a disease caused by the deposition of haemosiderin, which contains iron, from slow bleeding into the subarachnoid space [1]. It is a rare condition and a limited number of cases have been reported in the literature (270 cases reported between 1908–2006 [2]). T2*-weighted gradient echo sequences are sensitive to iron and can be used to inform the diagnosis of SS [3]. In this observational study of two superficial siderosis patients, quantitative susceptibility mapping (QSM) was used to perform longitudinal measurements of iron concentration in the brain as the patients underwent chelation therapy.

Methods. After surgical clipping to halt low-grade haemorrhages, the two patients had annual follow-up MRI scans on a Siemens Skyra 3T scanner. Acquisitions included an MPRAGE sequence and a gradient echo sequence with the magnitude and phase components saved. The MPRAGE images were used to produce brain masks and atlas-based segmentation was performed using Freesurfer. The phase images from the gradient echo sequence were used to calculate quantitative susceptibility maps (QSM), by unwrapping the phase, removing background fields using vSHARP and performing dipole inversion using iSWIM [4]. The QSM maps were registered to the baseline image and susceptibility values from the whole and edge of the cerebellum, brainstem and cortical ROIs were plotted as empirical cumulative distribution functions (eCDF), along with data from 10 control subjects for comparison.

Results. The susceptibility distributions changed more significantly with time for the two-voxel wide perimeter of the cerebellum (left) and brain stem (middle) masks compared to the whole masks. The susceptibility distributions changed more significantly with time for the superior temporal cortex ROI (right), chosen as it is adjacent to the sylvian fissure, compared to the whole cortex.



Discussion. Susceptibility values from regions most affected in the SS patients demonstrated a trend towards values in control subjects, suggesting that the chelation therapy was effectively removing haemosiderin deposits from the cerebral tissue in these regions. Other regions may not show a significant change in susceptibility distribution, as the affected volume of tissue is small compared to the total ROI.

Conclusion. The use of QSM as a potential clinical tool to monitor effects of iron chelation in superficial siderosis patients was demonstrated.

Key references.

1. Kumar N. Superficial siderosis: a clinical review. *Annals of Neurology*. 2021 Jun;89(6):1068-79.
2. Levy M, et al. Superficial siderosis: a case report and review of the literature. *Nature clinical practice Neurology*. 2007 Jan;3(1):54-8.
3. Kumar N. Neuroimaging in superficial siderosis: an in-depth look. *American journal of neuroradiology*. 2010 Jan 1;31(1):5-14.
4. Tang J, et al. Improving susceptibility mapping using a threshold-based k-space/image domain iterative reconstruction approach. *Magn Reson Med*. 2013; 69: p.1396–407.

Characterisation of a large plate of unknown magnetic shielding below a proposed MRI scanner room.

¹Schilling A, ¹Gregg JM, ¹Kumar A, ²Tang C, ³Collins M, ⁴Creaner J, ⁵Williamson S, ⁶Getty M, ⁶McCann AJ & ⁶McGrath C

¹ School of Mathematics and Physics, Queen's University Belfast, UK
² Gilligan Consulting Civil and Structural Engineers, 23 Bedford Street, Belfast, UK
³ Collins Rolston Architects, Causeway Tower, James Street South, Belfast, UK
⁴ Estates Department, Belfast Health & Social Care Trust, UK
⁵ Radiology Department, Belfast City Hospital, Belfast Health & Social Care Trust, UK
⁶ Northern Ireland Regional Medical Physics Service, Belfast Health & Social Care Trust, UK

Background

During the design phase to upgrade an MRI department, it was highlighted that an empty room previously used to house an MRI scanner had a large (7m × 5m × 15mm) metallic plate affixed 19 years previously, to the ceiling of the floor below to stop the 0.5mT magnetic flux density isosurface extending into the floor below. No details were available of the composition or properties of the large metallic plate. The MRI manufacturer required identification or characterisation before installation for impact on the new scanner and fringe field modelling. Removal was not an option.

Methods

Small core samples were taken from the corner of the shielding plate and imaged using electron microscopy. Targets from the electron microscopy image were selected for elemental analysis using Energy Dispersive (X-ray) Spectroscopy, EDS. The magnetic properties were determined using a Vibrating Sample Magnetometer, VSM. As these tests were carried out on microscopic samples, the MRI manufacturer required the density of the shielding material to incorporate into their modelling software. A 50mm x 50mm x 5mm section was prepared and weighed to determine the density.

Results

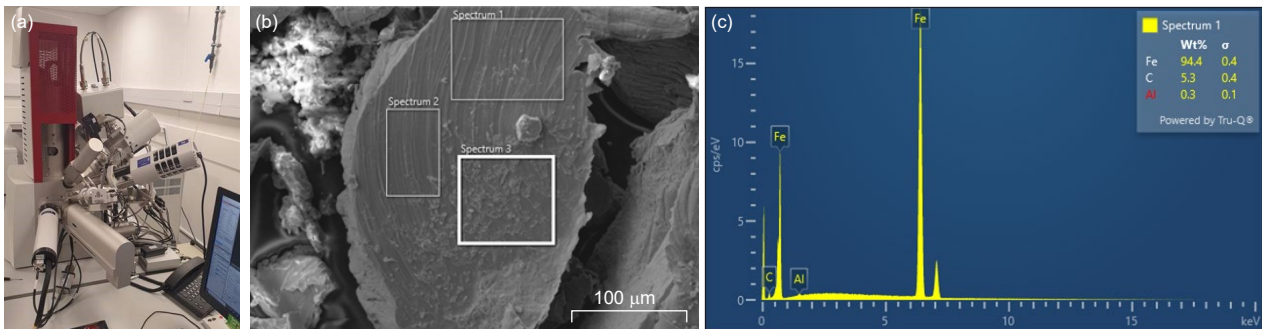


Figure 1: (a) EDS experimental set-up, (b) electron microscopy image of sample, (c) elemental analysis of sample.

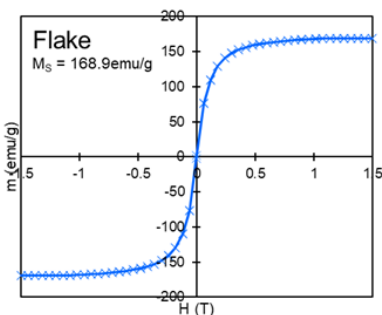


Figure 2: VSM results.

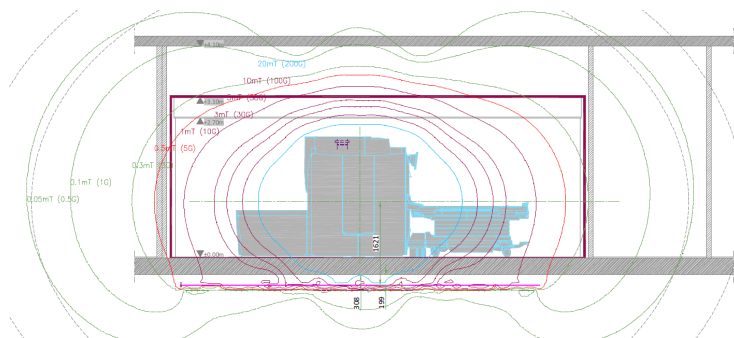


Figure 3: Site plan side view with modified fringe field incorporating shielding.

Discussion

Complex characterisation of samples of unknown magnetic shielding was carried out to enable incorporation into the magnetic fringe field modelling of the MRI scanner to be installed. The shielding had a density of $7830 \pm 50 \text{ kg/m}^3$ and magnetic properties similar to ARMCO DI-MAX M36 non-oriented electrical steel. Elemental analysis suggests it may be unrefined "pig iron" element. It was verified that the presence of the shielding can be accommodated by the shimming of the magnet during installation and theoretically, the 0.5mT safety isosurface (current UK legislative limit) does not extend appreciably into the floor below. This will be assessed experimentally post-magnet ramp-up. This study also highlights the need for detailed and accurate building construction records.

Development of a QA workflow for clinical quantitative diffusion imaging

Emily C. Kilgour, Mark Pether (NHS Grampian)

Background: Quantification of apparent diffusion coefficient (ADC) has many promising clinical applications, for example in identifying, staging, and quantitatively monitoring treatment response in prostate cancer. For ADC values to be meaningful clinically, they must be shown to be accurate and reproducible. QA of ADC values is particularly challenging in a clinical context because the values are temperature- and protocol-dependent. This work aims to design a suitable process for quality assurance of ADC values in a clinical context using a commercial diffusion phantom manufactured by CaliberMRI. The accompanying analysis software provided by Caliber was compared with software developed in-house.

Methods. The Caliber MRI diffusion phantom consists of 13 vials of different concentrations of water and PVP solution, and MR-readable thermometers. Caliber have also developed an accompanying piece of cloud software, qCal, which acquired diffusion images can be uploaded to for analysis. The qCal software requires the acquired diffusion to meet certain parameters and expects to receive four repeats of diffusion-weighted images for 5 b values (0, 500, 1000, 1500, 2000 $\mu\text{m}^2/\text{s}$). We optimised sequences which met the required parameters on a Siemens Avanto 1.5 T scanner using information provided by Caliber [1] and work undertaken by the NHS Greater Glasgow & Clyde MRI Group [2]. We then explored the suitability of the software for clinical QA.

Results & Discussion: After uploading the acquired images, the fully-automated qCal software creates an ADC map, volumes of interest are drawn to cover each vial and a report is produced. The report provides information on the mean ADCs acquired and how they compare with NIST ADCs, standard deviations, and SNR achieved for each diffusion weighting, among other quantities. However, the qCal software requires the sequence to conform to specified parameters, for example requiring specific b values, limiting the range of sequences which can be tested.

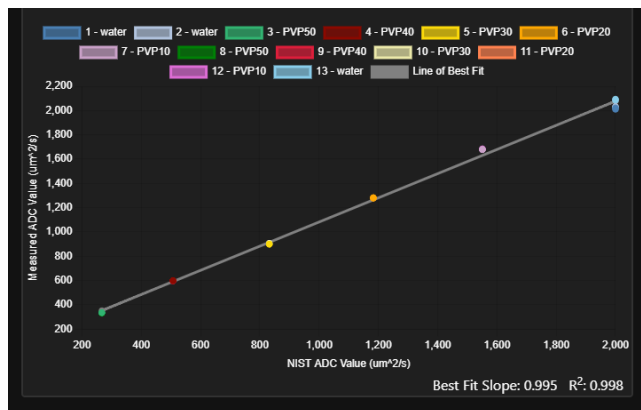


Figure 1: qCal comparison of measured and NIST ADC values.

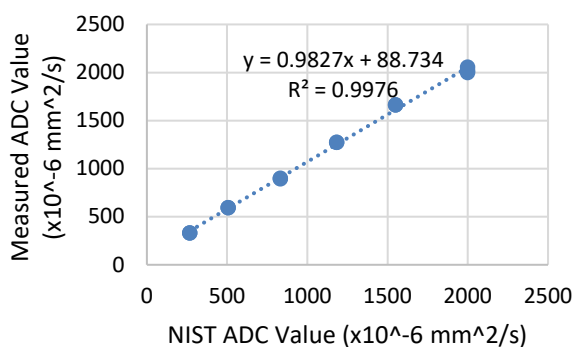


Figure 2: Analysis sheet comparison of measured and NIST ADC values.

For clinical use, we are particularly concerned with the accuracy and repeatability of ADCs. To allow assessment of the ADC values in our clinical sequences, we designed a workflow which uses ImageJ macros to extract data from any ADC map and an Excel sheet which analyses this data and produces relevant plots.

Figure 2 shows the same graph as Figure 1, created in our analysis sheet. The R^2 value on the slope was in agreement between the two methods. There was a small variation in the slope of around 1.2% between the methods but this may be a result of the ADC map calculation since the ADC map was calculated using qCal's

algorithm in Figure 1 and the Siemens algorithm used on the scanner in Figure 2.

Conclusion. Caliber MRI's software, qCal, is a valuable QA tool for comparing a scanner's ADCs with standardised NIST ADC values. However, its clinical functionality is limited and the main results of the software can be replicated using in-house software to a high degree of confidence.

Key Words: Quantitative MRI, DWI, ADC values, QA

[1] Caliber MRI. (2022) "Caliber MRI Diffusion Phantom" [Datasheet].

[2] B. Aylward. (2022). "Calibration of ADC values for quantitative MRI." University of Glasgow.

An RF cage can successfully attenuate radio waves from an RFID door security system so that it will not affect ³⁹K-MRI at 14MHz

Alan J. Wright^{1,2,3}, Elisabeth Pickles^{1,3}, Menglu Wu^{3,4}, Geoff Charles-Edwards^{1,2,3,5}, Özlem Ipek^{3,4}, and Jessica M. Winfield^{2,3,5}.

¹Guy's and St Thomas' NHS Foundation Trust; ² Department of Physics, The Royal Marsden NHS Foundation Trust, London, UK; ³London Collaborative Ultra High Field System (LoCUS), London, UK; ⁴School of Biomedical Engineering and Imaging Sciences, King's College London, London, UK; ⁵Division of Radiotherapy and Imaging, The Institute of Cancer Research, London, UK;

Background. An ultra-high field MRI at 7T (MAGNETOM Terra; Siemens Healthineers, Erlangen, Germany) can be used for potassium (³⁹K) imaging at 13.9MHz [3,4]. Potassium ions are concentrated in the intra-cellular space where their relative concentrations are potential indicators of a variety of pathological processes [2]. Radiofrequency identification (RFID) systems, which have active readers and passive tags, are often used as key/lock systems for doors to secure areas such as MRI control rooms. The powered reader, which is usually placed in a fixed location such as on a wall, actively transmits RF which interacts with the passive circuitry of the tag located in the key card, allowing communication by backscattering. A system operating at the RFID 'High Frequency' of 13.6MHz has the potential to provide a source of RF interference for potassium MRI at 7T.

Methods. 13.6MHz signal attenuation was measured using apparatus recommended in the IEEE standard 299[1] with two 0.3m diameter electrostatically shielded loops (ESL) as send and receive antennae. An APSIN2010 signal generator (Ana Pico, Switzerland) was used with a RAMP01M03GC Microwave System Amplifier (RF Lambda, TX-USA) to send RF which was received and detected with a FSH4 Spectrum Analyser (Rohde & Schwarz, Germany). A continuous wave signal at 13.6MHz, -3dB was generated and amplified. The receive loop was placed at distances from the send ESL of 7cm (the thickness of the RF cage door) and 67cm (as the standard [1]). Detection was performed with the spectrum analyser on a decibel scale over a 20kHz bandwidth. Attenuation was calculated as the decibel difference between through-air transmission and across the RF cage door. A 10cm diameter single loop coil was also built, tuned and matched to 13.6MHz, 50Ω to act as a resonant signal detection coil.

Results. The 7T MRI has a direct line between its isocentre and an RFID reader, which passes through the RF cage doorway. Placing the receive ESL next to the RFID antennae detected a signal of -7dB against a background of -111dB though this fell to -49dB 30cm away from the reader. Inside the scanner room no signal from the RFID could be detected with either the ESL or the 10cm tuned receive coil when the RF cage door was shut. This was over a distance of more than 3m. Transmitting through the closed-RF cage door - a 7cm separation between the ESL - a small signal could be detected which corresponded to 84.5dB of attenuation. Repeating this measurement with a 67cm separation led to no detectable signal across the closed RF door and the through air signal was 26.3dB attenuated, compared to a 7cm separation.

Conclusion. An attenuation of 80-100dB, as achieved here at 13.6MHz, is in the recommended range [1] for RF cage performance. RFID radio waves cannot be detected by tuned coils or ESL from inside the RF cage which is more than sufficient to shield RF coils from this source of contaminating signal.

Key words. Potassium MRI, UHF MRI, RF Engineering.

Key References. [1]IEEE -299 - IEEE Standard Method for Measuring the Effectiveness of Electromagnetic Shielded Enclosures (2006) ISBN 0-7381-5215-3. [2]Gast LV, Baier LM, Chaudry O, Meixner CR, Müller M, Engelke K, Uder M, Heiss R, Nagel AM. NMR Biomed. 2023 Jan;36(1):e4819. doi: 10.1002/nbm.4819. [3]Umatham R, Rösler MB, Nagel AM. Radiology. 2013 Nov;269(2):569-76. doi: 10.1148/radiol.13130757. [4] Wu M, McElroy S, Stark H, Charles-Edwards C, Winfield JW, Wright A, Ipek O. Proceedings of the ISMRM 2024, 1584.

Evaluating the Reproducibility of Radiomic Features with AIR Recon DL: A Phantom-Based Analysis

Edward J Peake¹, Joao G Duarte², Andrew N Priest^{1,2}, and Martin J Graves^{1,2}

¹Imaging, Cambridge University Hospitals NHS Foundation Trust, Cambridge, United

Kingdom, ²Department of Radiology, University of Cambridge, Cambridge, United Kingdom

Background. The Image Biomarker Standardization Initiative (IBSI) has done much to establish a general radiomics image processing scheme for calculation of features from imaging¹. The lack of standardized imaging protocols and wide variability between centres accentuates reproducibility challenges². MRI phantoms have been used for radiomic repeatability studies³, with good agreement to in-vivo findings⁴. In this study, we examine the effect of AIRTM Recon DL⁵, a Deep Learning (DL) reconstruction algorithm from GE Healthcare, on the consistency of radiomic features using phantoms with different radiomic characteristics.

Methods. MRI phantoms were developed with hypointense materials with diameters from 2mm to 5mm. The materials were mixed with agar, prepared following the Stanford Agar Phantom Recipe⁶, and poured into 50mm diameter glass vials. These phantoms were imaged using 2D Fast Spoiled Gradient Echo MRI with a range of NEX (number of average) and DL levels of 'Off', 'Low', 'Medium' and 'High'.

Three dimensional regions of interest were segmented, with each vial in the phantom assigned a separate label. Radiomic features were generated using Pyradiomics v3.1.0⁷ using the original parameter file. SNR was calculated for each NEX and DL Recon Level using method 1 from NEMA MS-1⁸. The intraclass correlation coefficient (ICC) was used to compare the features at each NEX and DL Recon level, at an approximately matched SNR of 40.

Results

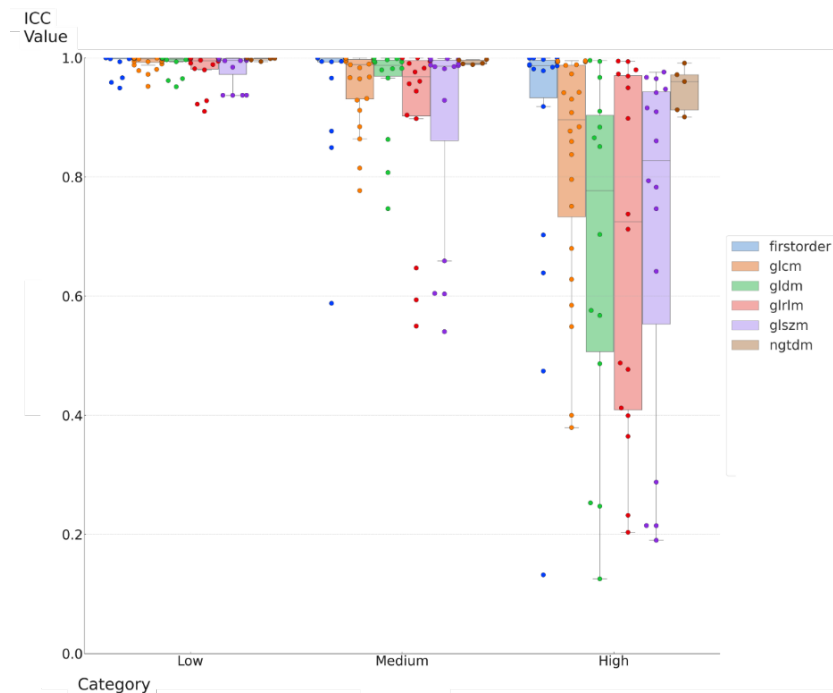


Figure 1: Interclass correlation coefficient (ICC) for radiomic features at matched SNR of approximately 40. Recon DL levels: High at NEX2, Medium at NEX4 and Low at NEX7 were compared to Recon DL level Off at NEX9. The ICC mean and standard deviations at each ARDL level were: Low 0.98 ± 0.05 , Medium 0.90 ± 0.18 , and High 0.63 ± 0.34 .

Discussion. ICC values were all excellent (>0.9) for all radiomic features at DL Low, while the proportion of radiomic features with $ICC > 0.9$ decreased to 83% and 58% for DL Medium and DL High respectively.

Conclusion. The reconstruction of images using AIRTM Recon DL has to potential to significantly affect radiomic features.

Key references. (1) [Radiology 295.2 \(2020\): 328-338](#), (2) [Medicinal Research Reviews 42.1 \(2022\): 426-440](#), (3) [Medical Physics. 2018 Feb 1;45\(2\):773–82](#), (4) [Scientific Reports 2021 11:1](#), (5) [arXiv preprint arXiv:2008.06559 \(2020\)](#) (6) [Lucas Center Agar Phantom Recipe](#), (7) [Cancer research 77.21 \(2017\): e104-e107](#), (8) [NEMA Standards Publication MS 1-2001 \(2001\)](#)

Does slice orientation affect spatial resolution when using SMS?

Aimon Qazi, Mark Pether (NHS Grampian)

Background. Simultaneous multislice imaging (SMS) is an advanced acceleration technology that utilises parallel imaging in order to reconstruct images from multiple slice excitations [1]. There is anecdotal evidence within the MRI physics community that SMS image quality is inferior in certain planes and oblique angles, particularly when imaging in the abdomen and pelvis. This work aimed to investigate if there is a measurable decrease in spatial resolution with slice orientation when various SMS acceleration factors are applied.

Methods. The spatial resolution magNET phantom was positioned at different angles using foam blocks and imaged using a TSE sequence with varying SMS factors (from 0 – 4). Image analysis was conducted using the ImageJ software. The modulation transfer function (MTF) was calculated from the central MTF block and the modulation of the 0.5mm line pairs in the phase and frequency encoding direction were also calculated and compared.

Results. Using the MTF's, the spatial frequency of the MTF 50 and MTF 10 values were compared for no SMS factor (S0) and an SMS factor of 4 (S4):

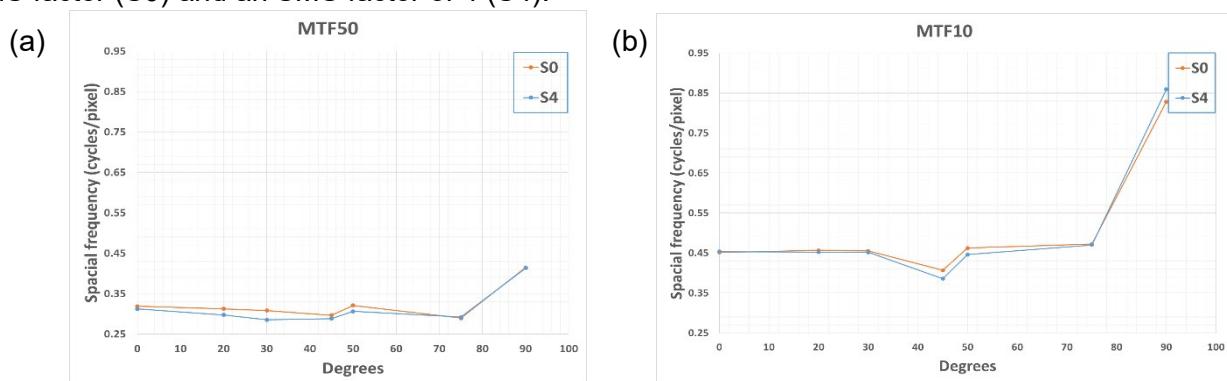


Figure 1: Spatial frequency values at (a) - 50% of the MTF (MTF50) and at (b) - 10% of the MTF (MTF10) versus the angle of tilt of the phantom, comparing no SMS (orange) and an SMS value of 4 (blue).

The modulation of the 0.5mm spaced line pairs in the phase and frequency encoding were calculated and compared:

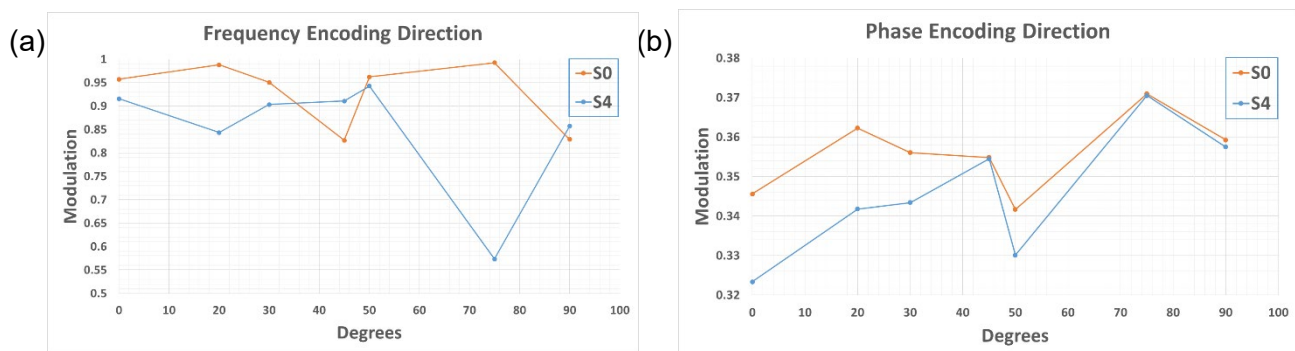


Figure 2: Average modulation of 0.5mm spaced line pairs versus the degree of phantom tilts at an SMS factor of 0 & 4 in the (a) - frequency, and (b) - phase encoding directions.

Discussion. Figure 1 shows up to a 7.4% reduction in spatial resolution at the MTF50 value and up to a 5% decrease at the MTF10 value. Furthermore, from Figure 2 the frequency encoding results are inconclusive, whereas the modulation in the phase encoding direction for SMS factor 4 remains consistently lower than the same pulse sequence without the use of SMS up to a difference of 6.4%.

Conclusion. There appears to be some degradation of spatial resolution particularly in the phase encoding direction when SMS is used. Oblique slices tend to produce worse resolution by the metrics considered in this work. Future work will investigate the relationship between these image quality metrics and lower SMS factors which are more commonly seen in routine practice.

Key references. [1] Barth M, Breuer F, Koopmans PJ, Norris DG, Poser BA. Simultaneous multislice (SMS) imaging techniques. *Magn Reson Med*. 2016 Jan;75(1):63-81. doi: 10.1002/mrm.25897. Epub 2015 Aug 26. PMID: 26308571; PMCID: PMC4915494.

Measuring the dimensions of structures within the ACR Large MRI QA phantom using CT

Jasmine Lister, Stephen Powell, Tom Vasey, Matt Hill, Alex Goodall, Andrew Fry
Sheffield Teaching Hospitals NHS Foundation Trust

Background.

IPEM 112 recommends performing scanner QA using a test object such as the ACR Phantom [1]. AT STH, we use the ACR phantom to perform six-monthly scanner QA, and values for parameters such as linearity, distortion, slice positioning, and slice thickness are calculated from the acquired images [2,3]. Tolerances for these parameters are set relative to ACR-quoted dimensions. The aim of this work was to measure the main structures within the phantom from CT images and compare the measured values to those quoted by ACR [3].

Methods.

Three ACR phantoms owned by the Trust were imaged on a Canon Aquilion One, using a routine Helical Brain protocol (slice thickness 0.5 mm; matrix size 512 x 512 and reconstruction diameter 220.312 mm giving a pixel size 0.43 mm².)

The reconstructed coronal, sagittal and transverse images were imported into Image J. The linear and angular calliper tools were used to measure the diameter, length and ramp angles, along with the distortion grid height and width. The ramp angles were also calculated trigonometrically using measured ramp height and lengths.

To reduce bias, the operator performed each measurement once in turn before waiting a short period and repeating five times. The values were collated across four operators (from the MR Physics team) and tabulated. The average measurement between all operators was then compared to the expected value.

Results.

Table 1 shows the average values for each measurement, averaged across all four operators for each of the individual phantoms, along with the standard deviation and the percentage difference between the average measurement and the quoted values by ACR.

Table 1: Average of each measurement, standard deviation and % difference from expected value for three phantoms.

Measurement	Declared ACR Value	Phantom and ID								
		RHH: J11468			NGH: J8736			WPH: J8764		
		Measured	Error (SD)	Difference	Measured	Error (SD)	Difference	Measured	Error (SD)	Difference
Diameter (mm)	190	189.56	0.47	-0.23%	189.47	0.46	-0.28%	189.73	0.43	-0.14%
Length (mm)	148	147.41	0.36	-0.40%	147.23	0.53	-0.53%	146.98	0.44	-0.69%
Ramp 1 Angle Calculated (°)	5.71	5.64	0.06	-1.27%	5.87	0.13	2.68%	5.85	0.09	2.39%
Ramp 1 Angle Measured (°)	5.71	5.72	0.07	0.13%	5.98	0.13	4.54%	6.02	0.18	5.22%
Ramp 2 Angle Calculated (°)	5.71	5.75	0.09	0.65%	5.87	0.09	2.69%	6.00	0.11	4.81%
Ramp 2 Angle Measured (°)	5.71	5.77	0.18	1.05%	5.94	0.25	3.83%	6.04	0.18	5.46%
Height Grid (mm)	150	152.32	0.80	1.52%	152.20	1.07	1.45%	152.51	0.88	1.65%
Width Grid (mm)	150	151.48	1.05	0.98%	151.88	0.64	1.24%	151.64	1.05	1.08%

Discussion.

The phantom diameter and length have a consistently low difference across all three phantoms and are of the same magnitude as the CT image pixel sizing. Therefore, these are not going to have a significant effect on the accuracy of any linearity or distortion measurements. The ramp angle measurements show high variability in difference across all three phantoms, so this should be taken into consideration when calculating slice widths. The grid height and width measurements show low variation in difference between phantoms but are consistently larger than the difference in diameter and length. This should also be considered if the distortion grid is used in QA.

Conclusion.

The difference between the measured and expected phantom diameter is less than the tolerance used in the linearity measurement. However, the difference between measured and expected grid size is much larger and could impact qualitative distortion measurements.

Key references.

[1] McRobbie, D., and S. Semple. "IPEM Report 112: Quality Control and Artefacts in Magnetic Resonance Imaging." (2017).

[2] Clarke, Geoffrey D. "Overview of the ACR MRI accreditation phantom." MRI Phantoms & QA Testing (1999): 1-10.

[3] ACR. "Phantom test guidance for the ACR MRI Accreditation Program." Am. Coll. Radiol. (2005): 5.

Title of Study**An MR Core Lab to support validation, quality assurance and evaluation of quantitative MR imaging biomarkers.**

¹*Markus J., ²*Keaveney S., ³Birchall J., ⁴Gallagher E., ³Gill A., ⁵Young, J.D., ¹Brew-Graves C., ¹Caselton L., ²Doran S.J., ¹Punwani S., ⁷Aboagye, E.O. and ⁶Hubbard Cristinacce P.L.

¹University College London, ²The Royal Marsden Hospital & The Institute of Cancer Research, ³University of Cambridge, ⁴University of Oxford, ⁵King's College London, ⁶The University of Manchester, ⁷Imperial College London. *Joint first authors/presenters

Background.

Quantitative MR Imaging Biomarkers (qMRIBs), require technical and clinical validation to ensure that the technique can perform across the varied UK MR landscape and be adopted successfully into healthcare provisions¹. Successful validation includes evaluation of reproducibility according to metrological principles². This is hampered by variability in quality assurance and quality control practices across the UK², both in terms of image acquisition and analysis. There is a pressing need for standardised quality management in imaging studies to support qMRIBs towards adoption as meaningful clinical tools.

Methods.

The National Cancer Imaging Translational Accelerator (NCITA)⁴ was established in 2019 with the primary aim of providing support, guidance and infrastructure to develop qMRIBs from incomparable, single centre, based metrics into reproducible, vendor agnostic, quality-assured imaging toolkits. Specifically, NCITA provides practical support for qMRIBs through the MR Core Lab (MRCL)⁵. MRCL continuously develops and reviews pathways to benefit qMRIB validation, as well as working with study teams to offer bespoke services. MRCL engages with study teams and other 3rd party services to provide guidance in ways to increase QC and QA reports of data from study design, multi site activation to analysis.

Results

The MRCL evaluates imaging protocols to ensure all sites are capable of maintaining data integrity. Harmonised imaging protocols are created through a process of technical imaging review, which ensures technical performance, data workflow, and staff training is sufficient to provide good quality data. A quality management system is used to monitor sites, equipment and processes. Anonymised imaging data are reviewed and the MRCL provides a combined manual and automated assessment of imaging data quality.

Discussion.

MRCL supports validation with end-to-end quality management in study set-up, image acquisition and analysis. We propose that this service can provide critical links to improve evaluation of qMRIBs.

Key references.

[1] O'Connor, JPB. et al. *Nat. Rev. Clin. Oncol.*, 14(3), p169-86, 2017; [2] Hubbard Cristinacce, PL. et al. *Phys. Med.*, 101, p165-82, 2022; [3] Cashmore, MT. et al. *Br. J. Radiol.* 94(1120), 2021; [4] McAteer, M. et al. *Br. J. Cancer.* 125(11), p1462-65, 2021; [5] <https://ncita.org.uk/ncita-mr-core-lab/>

A Survey of Faraday Cage Attenuation Measurements of New Clinical MRI Systems

Jamie Small, David Price, Francesco Padormo, Joe Martin, Alan Wright, Anthony Price, Jane Ansell, Elizabeth Gabriel, Laurence Jackson, Simon Shah, Caitlin O'Brien, Geoff Charles-Edwards

Background. Scanner manufacturers typically specify new MRI systems to have a minimum Faraday Cage (FC) attenuation of 90-100dB prior to installation [3,4] and IEEE standard 299-2006 recommends an 80-100dB attenuation to avoid RF interference in electronic equipment [1]. Our experience has suggested that new FCs tested independently at acceptance can already be below 80dB due to minor damage to the RF cage during installation. We present a survey of FC attenuation measurements across 34 brand new MR systems immediately prior to client handover in order to gain insight into realistic values of FC performance once in routine clinical use.

Methods. Measurements were performed according to IEEE 299-2006 [1] utilising adjustable dipole antennae arms for transmission and reception at 65MHz, 128MHz & at 297MHz. RF power transmission through the FC was subsequently measured at typical locations of FC vulnerability; at the console room window, the magnet room door, and the penetration panel (PP). FC attenuation measurements were acquired on 34 MRI systems over 7 years (2017-2024) as part of acceptance testing. These measurements were then added to available historic data [2] to analyse the dependence of cage performance on scanner age using Spearman's Test. RF noise image tests were also carried out as part of acceptance testing to detect any RF interference.

Results. The median FC attenuation at all measurement locations at acceptance testing were within the IEEE range up to 128MHz (Figure 1), however a large variance was observed with 11/34 scanners having at least one measurement below 80dB at its' resonant frequency. Across all sites and frequencies, all three measurement locations demonstrated roughly equal attenuation. Spearman correlations indicated that there is a significant large negative relationship between the age of the scanner and attenuation of the door ($r(46) = -0.658, p < 0.001$) and window ($r(46) = -0.65, p < 0.001$). No RF interference was noted in any image tests for any of the scanners at acceptance.

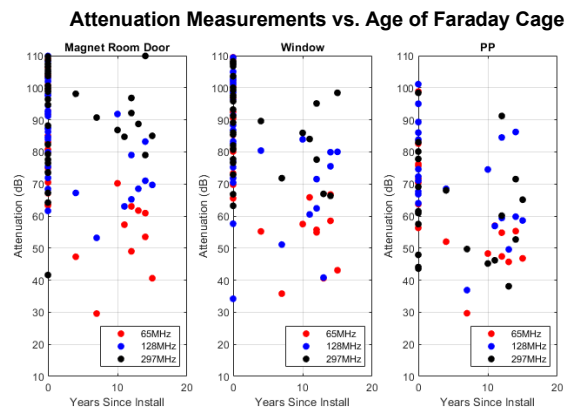
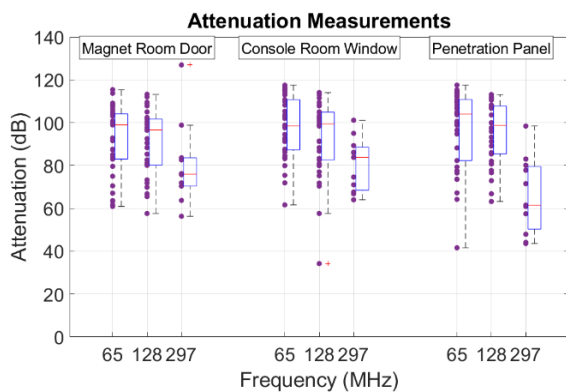


Figure 1: FC attenuation measurements of 34 clinical MRI systems at acceptance test. Figure 2: FC Attenuation measurements vs. FC age measured at three locations.

Discussion. 11/34 scanners had at least one measurement below the IEEE specification at resonant frequency. Below 50dB we have observed interference between two side by side clinical scanners operating simultaneously with wide transmit and receive bandwidth sequences. We expect the strong negative relationship between cage age and window attenuation to be more reflective of the door rather than the RF window, which is unlikely to change with time.

Conclusion. This work shows that having a check of RF cage performance after scanner installation can be helpful if FC attenuation has been reduced during the install process. General degradation may further reduce performance and where a significant source of external interference is present it may lead to RF artefacts.

Key references. 1. IEEE -299 - IEEE Standard Method for Measuring the Effectiveness of Electromagnetic Shielded Enclosures. 2. Padormo, Martin, Ansell, et al. Proc. ISMRM 2021 3. Phillips Planning Guide, page 14. 4. Planning Guide Vida, page 237

Evaluation of UKCA marked fMRI software

¹Johnston B, ¹Allwood-Spiers S, ²Logan J, ²Donnelly P, ²Macdonald K, ²Fullerton NE

¹MRI Physics, NHS Greater Glasgow and Clyde (NHS GG&C), UK, ²Neuroradiology, Institute for Neurological Sciences, NHS GG&C, UK

Background. The clinical fMRI service in NHS Greater Glasgow and Clyde (NHS GG&C) was established over 20 years ago. The analysis software that has been used by the MRI Physics team for the majority of this time includes FSL (FMRIB Software Library) scripts. This software has not been approved for clinical use and is not CE or UKCA marked as a medical device. When the 3T MRI scanner used for clinical fMRI was replaced, Siemens Neuro 3D software was purchased. This Siemens software is able to perform fMRI analysis, and has CE and UKCA marking as a medical device. An audit is currently being performed to evaluate the output of FSL, Siemens or using both in combination.

Methods. Three Neuroradiologists will be asked to report clinical fMRI images, one using FSL output only, another using Siemens output only, and the third using output from both software. Each category will be spread evenly among the Neuroradiologists. The Neuroradiologist using both software packages will produce the clinical report.

Results. The audit is currently ongoing. Our initial observations that led us to perform this audit were apparent differences in the image registration and the resultant haemodynamic activation observed between the two analysis software packages. The audit aims to formally assess this and ascertain whether these differences could be clinically relevant for interpretation of the fMRI results.

Discussion. A UK equivalent to the EU Medical Devices Regulations is expected to be introduced in the near future. Many clinical fMRI sites are using software that is not CE or UKCA marked as a medical device. If it is found that non-CE/UKCA marked software performs significantly better, then an exemption may be required.

Conclusion. An IPEM task and finish group looking to collaborate and share best practice in running a clinical fMRI service has been proposed. By pooling our shared experience, it will allow us to provide the best possible service for our clinical fMRI patients.